Editors' Suggestion

Nanosecond Melting and Recrystallization in Shock-Compressed Silicon

Stefan J. Turneaure,[1] Surinder M. Sharma,[1] and Y. M. Gupta[1,2]
[1]*Institute for Shock Physics, Washington State University, Pullman, Washington 99164, USA*
[2]*Department of Physics and Astronomy, Washington State University, Pullman, Washington 99164, USA*

(Received 22 May 2018; revised manuscript received 10 July 2018; published 25 September 2018)

In situ, time-resolved, x-ray diffraction and simultaneous continuum measurements were used to examine structural changes in Si shock compressed to 54 GPa. Shock melting was unambiguously established above ∼31–33 GPa, through the vanishing of all sharp crystalline diffraction peaks and the emergence of a single broad diffraction ring. Reshock from the melt boundary results in rapid (nanosecond) recrystallization to the hexagonal-close-packed Si phase and further supports melting. Our results also provide new constraints on the high-temperature, high-pressure Si phase diagram.

DOI: 10.1103/PhysRevLett.121.135701

Shock compression experiments—because they can access very high-pressures and high-temperatures—are well suited for examining material phase diagrams [1], including the melt boundary, that are not easily accessed using static experiments. As such, shock compression experiments have provided unique insights into condensed matter states under extreme conditions including iron at earth core conditions [2,3], carbon phases at TPa pressures [4], and silica at planetary interior conditions [5]. Although shock-induced phase transformations, particularly those resulting in large volume changes, can be detected using continuum measurements [1], such measurements do not provide structural information for the high-pressure phase. *In situ*, x-ray diffraction (XRD) measurements have been crucial for identifying high-pressure structures in shock-induced solid-solid phase transformations [6–11]. In contrast, melting, a fundamental and extensively studied phase transition in materials, is more challenging to examine under shock compression, in part, because the volume change associated with melting is often small, and also because XRD patterns from liquids and from amorphous solids are not easily distinguished.

Although the possibility of melting under shock compression has long been recognized [1,12], inferences of shock melting have largely been indirect. Early inferences relied on the observation of discontinuities in shock velocity vs particle velocity data [1,13]. Sound speed discontinuities have also been used as a signature of shock melting since the liquid phase is expected to have no shear modulus [2]. Melting has also been inferred through the observed plateau (ascribed to latent heat) in the increase of temperature with stress [3,5,14]. Recently, efforts have been made to identify melting using XRD in nanosecond duration laser shock experiments on Mo [15], Sc [16], and Bi [17]. These conclusions are essentially based on observation of weakening and broadening of a single diffraction line and are, therefore, not unambiguous. Direct and unequivocal demonstration of shock melting remains an important objective. For that, several sharp XRD lines, signifying crystallinity, must all vanish and the issue of amorphization rather than melting needs to be carefully addressed. Similarly, crystallization of shocked liquid phases is of fundamental importance to gain insights into the crystallization kinetics in real time.

Here, we report on *in situ*, time-resolved, XRD measurements in plate impact experiments to examine the structure of shock-compressed silicon along the Hugoniot between 26–54 GPa—providing explicit proof of shock melting through the simultaneous vanishing of all sharp crystalline diffraction peaks above ∼33 GPa. Recrystallization of liquid Si observed upon reshock and during release from the Hugoniot state on nanosecond timescales makes a persuasive case for melting rather than amorphization.

Under static compression at ambient temperature, Si undergoes six structural transformations [18]. With increasing temperature at ambient pressure, the cubic diamond (cd) phase melts without undergoing any other phase transitions. The melting temperature of cd Si decreases with pressure [19] up to the cd–β-tin–liquid triple point near 1000 K and 11 GPa [20,21] and increases slightly for higher pressures [21]. Measured Si phase boundaries including the melting curve have not been reported for elevated temperatures above ∼16 GPa.

Although previous shock-compression experiments have driven Si into high-temperature, high-pressure states, most diagnostics have been insufficient to determine the structure or phase boundaries [22–28]. Early continuum studies concluded that a large volume change (>20%) occurs somewhere above ∼10 GPa [22–24] consistent with a transformation to a high-pressure Si structure [18]. Subsequently, the structure of Si shocked to 26 GPa was confirmed to be simple hexagonal (sh) using *in situ*, XRD measurements [8]. Based on characterization of

 © 2018 American Physical Society

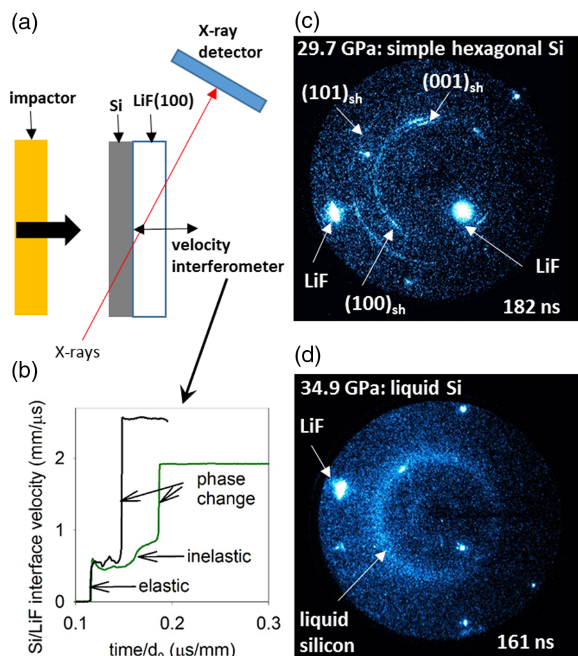

FIG. 1. (a) Configuration for simultaneous *in situ*, XRD, and continuum measurements in shock compressed Si. (b) Representative Si/LiF velocity histories for impact stresses of 32.7 and 47.8 GPa. For impact stress larger than 39 GPa, the phase transformation wave overdrives the inelastic shock. (c) and (d) Representative XRD patterns recorded from shocked Si (100). LiF impactors and windows were (100) oriented single crystals and the LiF(100) Laue XRD spots were masked before integrating diffraction patterns azimuthally. Times listed in XRD patterns are relative to impact.

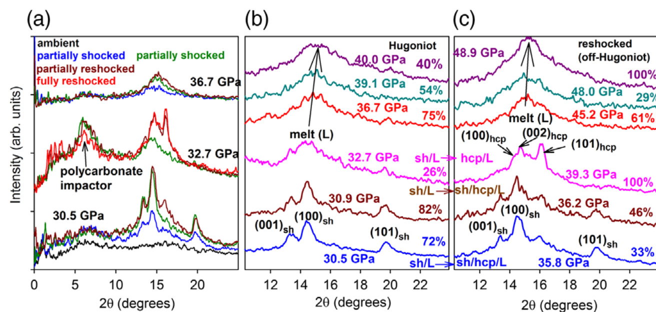

FIG. 2. Representative XRD line profiles recorded for shocked Si(100). (a) Time evolution of XRD line profiles (153.4 ns between profile measurements; green profiles obtained one frame after blue profiles) from three experiments. Stresses listed are impact stresses. (b) XRD patterns corresponding to Si(100) on the Hugoniot with impact stresses and percentage of Si(100) through which the phase transformation wave has propagated listed. (c) XRD patterns corresponding to partially or fully reshocked Si(100) with reshock stresses and percentage of Si reshocked listed. Line profiles with matching colors in panels (b) and (c) were obtained in the same experiment.

Si recovered following laser-shock compression and associated MD simulations, it was suggested that Si amorphizes during shock compression [28]. Other MD simulations have either predicted a transformation to the Imma phase before melting at ∼36 GPa [29] or have provided Hugoniot states for shock-compressed Si [30]. However, to date, shock melting and crystalline structures other than sh have not been observed *in situ*, in shock-compressed Si.

In the present experiments, shock-compressed Si was examined using the configuration shown in Fig. 1(a). Upon impact of a flyer plate (LiF or polycarbonate) onto a Si sample (0.5–1.6 mm thick), three waves—corresponding to elastic, inelastic, and phase transformation response—propagate through the Si; wave profiles were recorded using a velocity interferometer at the Si/LiF interface (see Figs. 1(b), and S2 and S3 of the supplementary materials [31]). Analysis of the transmitted wave profiles provided the stress and density on the Hugoniot [31]. Corresponding Hugoniot temperatures were obtained from Ref. [30]. Off-Hugoniot Si states were achieved after the phase transformation wave reflected as a reshock from the Si/LiF interface and/or at late times after stress release. Reshock stresses were obtained directly from the measured Si/LiF interface velocity and the LiF Hugoniot [34]. Specific parameters for each experiment are provided in the Supplemental Material, Tables S1–S3 [31].

The shock-compression experiments were performed at the Dynamic Compression Sector at the Advanced Photon Source using the 24-bunch synchrotron mode: ∼100 ps duration x-ray pulses every 153.4 ns. Time-resolved, powder XRD measurements (∼23 keV x-rays), recording four XRD frames each separated by 153.4 ns, were used to examine the structural evolution at different stresses along the Hugoniot, and for reshocked and/or released states. Silicon samples were either single crystal (shocked along [100]) or polycrystalline. Most experiments were performed on single crystal Si and we focus our discussion on those results. Results for polycrystalline Si are consistent with the Si(100) results [31].

Representative XRD data from shocked Si(100) for stresses near the melting transition are shown in Figs. 1(c) and 1(d). The partial Debye rings observed at 29.7 GPa correspond to a textured high-pressure crystalline structure, and the smooth broad diffuse ring observed at 34.9 GPa demonstrates loss of crystallinity. We identify the noncrystalline state as the liquid phase, and we provide further supporting evidence after presenting the experimental results.

Figure 2(a) shows the temporal evolution of XRD line profiles for shocked Si(100) for three representative experiments with peak stresses near the onset of shock melting (bottom), near the completion of shock melting (middle), and for complete shock melting (top). For 30.5 and 32.7 GPa impact stresses, crystalline diffraction peaks are apparent in the shocked and/or reshocked state, whereas for 36.7 GPa peak stress only a broad diffraction feature due to liquid Si is observed. Figures 2(b) and 2(c) show

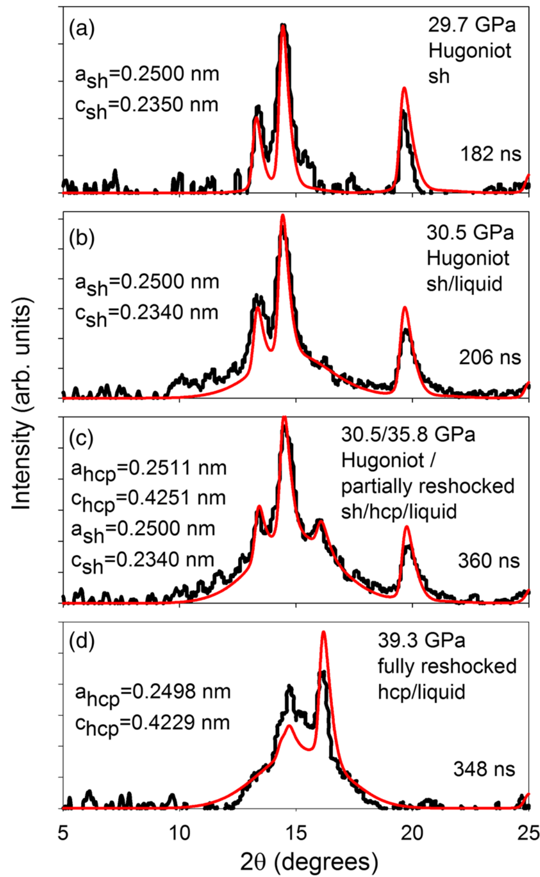

FIG. 3. Representative background-subtracted measured XRD line profiles (black lines) and simulated XRD line profiles (red lines) for Si(100). (a) For 29.7 GPa impact stress, the measured peaks match a sh diffraction simulation. (b) For 30.5 GPa impact stress, the measured peaks match a superposition of a sh diffraction simulation and a Gaussian representing liquid Si. (c) After partial reshock from 30.5 GPa impact stress to 35.8 GPa, the measured peaks match a superposition of sh and hcp diffraction simulations and a Gaussian representing liquid Si. (d) After reshock from 32.7 to 39.3 GPa, measured peaks match a superposition of a hcp diffraction simulation and a Gaussian representing liquid Si. Times listed in XRD patterns are relative to impact.

XRD line profiles for Si(100) corresponding to the Hugoniot and to the reshocked state, respectively.

The structure of shocked Si along the Hugoniot is determined from the XRD line profiles obtained prior to the phase transformation wave reaching the Si/LiF interface. For an impact stress of 29.7 GPa, the diffraction line profile is well matched by a diffraction simulation using the sh Si structure [Fig. 3(a)]. For impact stresses from 30.5–32.7 GPa, the line profiles have diffraction peaks characteristic of the sh Si structure and a broad hump due to liquid Si [Fig. 2(b)]. The diffraction profile for Si(100) shocked to 30.5 GPa matches the combination of a sh Si diffraction simulation and a Gaussian due to liquid Si [Fig. 3(b)]. For Si shocked to 32.7 GPa, the diffraction pattern is primarily a broad hump—with weak superposed sh Si peaks—indicating that melting is nearly complete. For impact stresses of 34.7 GPa and higher, only a broad diffraction hump was observed indicating complete melting during shock compression. From these findings, we conclude that the Hugoniot of shocked Si passes through the sh phase, intersecting the sh-liquid phase boundary from ∼30–33 GPa before undergoing complete melting.

The Si stresses and specific volumes along the Hugoniot, determined from the velocity interferometry data [31], are shown in Fig. 4(a). The solid-liquid transition from ∼30–33 GPa is not readily apparent from these continuum results, since the specific volume varies smoothly with shock stress through the melt transition. The sh Si specific volumes, calculated from the sh Si lattice parameters determined from XRD measurements [31], are in excellent agreement with the densities determined from the continuum measurements. Additionally, the Si Hugoniot calculated using QMD assuming a liquid final state [30] is consistent with continuum results at all peak stresses. These observations highlight the importance of the XRD measurements for identifying the melt transition in shock-compressed Si.

The reshocked states provide further insight into the Si phase diagram near the melt boundary. After reshock from states on the sh-liquid phase boundary, a new sharp (101) hexagonal close-packed (hcp) peak, in addition to a broad liquid Si hump, emerges near $2\theta = 16.2°$ showing that the reshocked Si has passed the sh-hcp-liquid triple point but remains on the melt boundary. For states due to reshock from 30.5 and 30.9 GPa to 35.8 and 36.2 GPa, respectively, both sh and hcp XRD peaks are observed; this is expected since the reshock wave has propagated through less than half of the Si thickness, and the measured line profiles are matched by a superposition of simulated line profiles for sh and hcp structures and a Gaussian representing liquid Si [Fig. 3(c)]. For complete reshock from 32.7 to 39.3 GPa, the sh peaks are no longer present and the observed line profile is matched by simulated hcp diffraction peaks and a Gaussian representing liquid Si [Fig. 3(d)]. The specific volumes of the hcp Si determined from the XRD data are shown in Fig. 4(a) and are consistent with the extrapolated hcp specific volumes from static compression of Si [38]. Crystalline diffraction peaks were not observed for Si reshocked from Hugoniot stresses of 36.7 GPa or higher indicating that the liquid-solid phase boundary was not crossed during reshock of pure liquid Si.

The velocity interferometry measurements were also used to calculate the reshock specific volume and stress after the phase transformation wave reflects from the Si/LiF interface [31]. The compressibility increases significantly during reshock from ∼30–33 GPa stresses (Figs. S6-S8) when the sh-hcp-liquid triple point is crossed on the melt line. In contrast, for lower peak stresses where reshocked sh Si remains sh and for higher peak stresses where reshocked

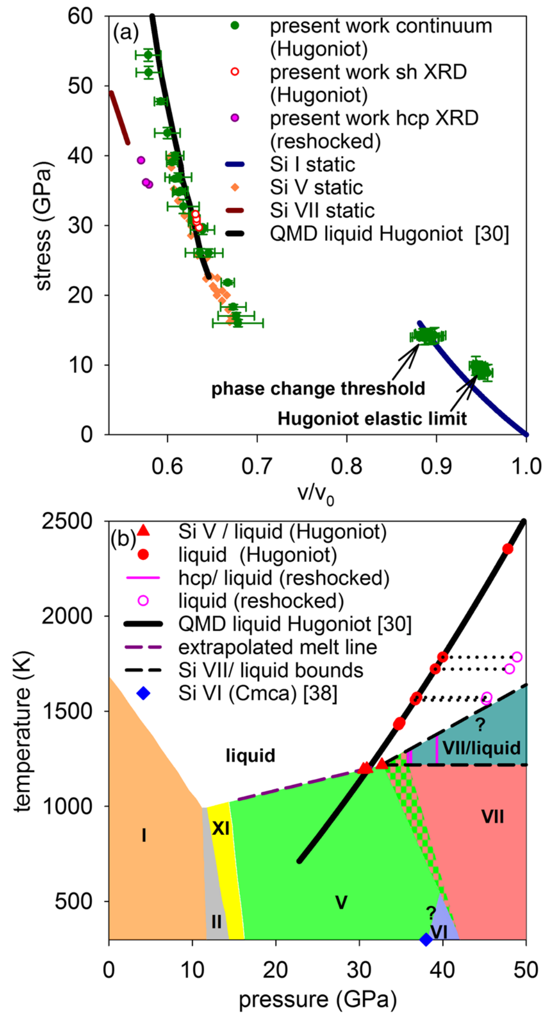

FIG. 4. Phase diagram for silicon. (a) Stress-volume results. The four lowest peak stress continuum Hugoniot results are from Ref. [26]. The blue line is for hydrostatically compressed cd Si based on second and third order elastic constants [41]. The Si V (sh) static compression data (orange diamonds) are from Refs. [38,42,43]. Si VII (hcp) static compression results from Ref. [38] are summarized by the dark red line. (b) Pressure-temperature summary. The phase boundaries between Si I (cd), II (β-tin), XI (Imma), V and the melt line up to 16 GPa are from Ref. [21]. Dotted lines connect Hugoniot and reshocked states from the same experiment. Temperatures for completely melted Si were obtained from calculations in Ref. [30].

liquid Si remains liquid Si, the volume change during reshock is significantly smaller (Fig. S8) [31]. Thus, the continuum results are well aligned with the XRD observations—transformation to the hcp structure during reshock occurs only when reshocked from the sh-liquid melt boundary.

Figure 4(b) summarizes our extension of the Si phase diagram to elevated temperatures above 16 GPa. The melting line previously measured between the cd–β-tin–liquid triple point and 16 GPa [20,21] is linearly extrapolated to the lower pressure bound (32.7 GPa) determined here for the sh-hcp-liquid triple point; the three Hugoniot stresses corresponding to sh-liquid mixtures are shown on this extrapolated melt curve. The sh-hcp phase boundary is constrained to intersect the melt curve between 32.7 and 35.8 GPa; the uncertainty in the phase boundary is indicated by the checkered region. At ambient temperature, the *Cmca*-hcp phase transition occurs at 42 GPa [38]; however, the *Cmca* structure was not observed in our shock experiments. Thus, we conclude that $dP/dT < 0$ for the sh-hcp phase boundary, and a *Cmca*-sh-hcp triple point exists somewhere below the melt boundary.

Past work does not provide guidance on the melt line for pressures above the sh-hcp-liquid triple point. We expect the hcp-liquid melt boundary to have $dP/dT > 0$, typical for close-packed metals [44]; thus, $dT/dP = 0$ provides a lower bound temperature estimate for the hcp-liquid phase boundary. An approximate upper bound for the hcp-liquid boundary is obtained from the reshock stresses at which complete melt was observed both on the Hugoniot and after reshock. The black dashed lines in Fig. 4(b) bracket the uncertainty range (cyan region) of the hcp-liquid melt line. The three reshocked states that exhibit a mixture of hcp and liquid Si are shown as pink vertical bars in the bracketed hcp-liquid phase boundary region.

In principle, the broad diffraction peaks observed from shock-melted Si could also be due to amorphization during shock compression. However, the monotonic increase of temperature with shock stress [30] is contrary to the kinetic impedance necessary to realize a structurally frustrated amorphous state [45]. Additionally, our observations of recrystallization during stress release from noncrystalline shocked states (see Fig. S17 [31]) and during reshock from a primarily noncrystalline state (from shock stress of 32.7 GPa) suggest that the kinetic barriers for crystallization are small (given the small temperature increase expected during reshock and the small temperature decrease during release). These findings provide strong supporting evidence that the noncrystalline state in shocked Si is liquid rather than a metastable amorphous solid, since large temperature increases are typically required to initiate crystallization of an amorphous solid to the ground state structure [11].

The local structure of liquid Si is reported to be similar to the crystalline β-tin structure from 0–8 GPa, before transforming to a denser liquid between 8–14 GPa [40,46]. The $Q = 4\pi \sin\theta/\lambda$ values of the center of the broad XRD humps observed for shock-melted Si are consistent with extrapolated values from lower pressure static data [40] (see Fig. S18) implying that liquid Si may be a three-dimensional network liquid even at higher pressures.

To summarize, our *in situ,* time-resolved, XRD measurements in shock-compressed Si show that all crystalline diffraction peaks vanish above ~33 GPa, providing unambiguous proof of shock melting. The present work is also unique in that Hugoniot and off-Hugoniot states were both

examined with *in situ* XRD in the same experiment allowing Si phase boundaries to be examined off the Hugoniot. Recrystallization of liquid Si was observed on nanosecond timescales during both reshock and during stress release. Such measurements provide a new approach for distinguishing between shock-induced melting and amorphization. Finally, our results provide new insight into the high-temperature, high-pressure Si phase diagram by constraining the sh-hcp-liquid triple point, by demonstrating that $dP/dT < 0$ for the sh-hcp phase boundary, and by constraining the hcp-liquid melt line.

J. M. Winey is thanked for carefully checking the continuum analysis and valuable discussions and comments regarding the manuscript. Yoshi Toyoda, Paulo Rigg, Adam Schuman, Nicholas Sinclair, and the DCS staff are thanked for assistance with the plate impact experiments. This publication is based upon work supported by the U.S. Department of Energy (DOE), National Nuclear Security Administration (NNSA) under Award No. DE-NA0002007. This publication is also based upon work performed at the Dynamic Compression Sector supported by the DOE/NNSA under Award No. DE-NA0002442 and operated by Washington State University. This research used resources of the Advanced Photon Source, a DOE Office of Science User Facility operated for the DOE Office of Science by Argonne National Laboratory under Contract No. DE-AC02-06CH11357.

[1] G. E. Duvall and R. A. Graham, Rev. Mod. Phys. **49**, 523 (1977).
[2] J. M. Brown and R. G. McQueen, J. Geophys. Res. **91**, 7485 (1986).
[3] C. S. Yoo, N. C. Holmes, M. Ross, D. J. Webb, and C. Pike, Phys. Rev. Lett. **70**, 3931 (1993).
[4] M. D. Knudson, M. P. Desjarlais, and D. H. Dolan, Science **322**, 1822 (2008).
[5] M. Millot, N. Dubrovinskaia, A. Černok, S. Blaha, L. Dubrovinsky, D. G. Braun, P. M. Celliers, G. W. Collins, J. H. Eggert, and R. Jeanloz, Science **347**, 418 (2015).
[6] T. d'Almeida and Y. M. Gupta, Phys. Rev. Lett. **85**, 330 (2000).
[7] D. H. Kalantar *et al.*, Phys. Rev. Lett. **95**, 075502 (2005).
[8] S. J. Turneaure, N. Sinclair, and Y. M. Gupta, Phys. Rev. Lett. **117**, 045502 (2016).
[9] S. J. Turneaure, S. M. Sharma, T. J. Volz, J. M. Winey, and Y. M. Gupta, Sci. Adv. **3**, eaao3561 (2017).
[10] P. Kalita, P. Specht, S. Root, N. Sinclair, A. Schuman, M. White, A. L. Cornelius, J. Smith, and S. Sinogeikin, Phys. Rev. Lett. **119**, 255701 (2017).
[11] S. J. Tracy, S. J. Turneaure, and T. S. Duffy, Phys. Rev. Lett. **120**, 135702 (2018).
[12] R. G. McQueen and S. P. Marsh, J. Appl. Phys. **31**, 1253 (1960).
[13] S. B. Kormer, M. V. Sinitsyn, A. I. Funtikov, V. D. Urlin, and A. V. Blinov, Sov. Phys. JETP **20**, 811 (1965).
[14] S. B. Kormer, M. V. Sinitsyn, G. A. Kirillov, and V. D. Urlin, Sov. Phys. JETP **21**, 689 (1965).
[15] J. Wang, F. Coppari, R. F. Smith, J. H. Eggert, A. E. Lazicki, D. E. Fratanduono, J. R. Rygg, T. R. Boehly, G. W. Collins, and T. S. Duffy, Phys. Rev. B **92**, 174114 (2015).
[16] R. Briggs *et al.*, Phys. Rev. Lett. **118**, 025501 (2017).
[17] M. G. Gorman *et al.*, Phys. Rev. Lett. **115**, 095701 (2015).
[18] A. Mujica, A. Rubio, A. Munoz, and R. J. Needs, Rev. Mod. Phys. **75**, 863 (2003).
[19] A. Jayaraman, W. Klement, and G. C. Kennedy, Phys. Rev. **130**, 540 (1963).
[20] V. V. Brazhkin, A. G. Lyapin, S. V. Popova, and R. N. Voloshin, Phys. Rev. B **51**, 7549 (1995).
[21] A. Kubo, Y. Wang, C. E. Runge, T. Uchida, B. Kiefer, N. Nishiyama, and T. S. Duffy, J. Phys. Chem. Solids **69**, 2255 (2008).
[22] M. N. Pavlovskii, Sov. Phys. Solid State **9**, 2514 (1968).
[23] W. H. Gust and E. B. Royce, J. Appl. Phys. **42**, 1897 (1971).
[24] T. Goto, T. Sato, and Y. Syono, Jpn. J. Appl. Phys. **21**, L369 (1982).
[25] A. Loveridge-Smith *et al.*, Phys. Rev. Lett. **86**, 2349 (2001).
[26] S. J. Turneaure and Y. M. Gupta, Appl. Phys. Lett. **91**, 201913 (2007).
[27] A. Higginbotham *et al.*, Sci. Rep. **6**, 24211 (2016).
[28] S. Zhao, E. N. Hahn, B. Kad, B. A. Remington, C. E. Wehrenberg, E. M. Bringa, and M. A. Meyers, Acta Mater. **103**, 519 (2016).
[29] G. Mogni, A. Higginbotham, K. Gaal-Nagy, N. Park, and J. S. Wark, Phys. Rev. B **89**, 064104 (2014).
[30] O. Strickson and E. Artacho, Phys. Rev. B **93**, 094107 (2016).
[31] See Supplemental Material at http://link.aps.org/supplemental/10.1103/PhysRevLett.121.135701 for additional experimental details, additional velocity interferometry results, analysis of velocity interferometry data to obtain stress and density and additional XRD results and analysis details. Supplemental Material includes Refs. [32–40].
[32] O. T. Strand, D. R. Goosman, C. Martinez, T. L. Whitworth, and W. W. Kuhlow, Rev. Sci. Instrum. **77**, 083108 (2006).
[33] L. M. Barker and R. E. Hollenbach, J. Appl. Phys. **43**, 4669 (1972).
[34] Q. Liu, X. Zhou, X. Zeng, and S. N. Luo, J. Appl. Phys. **117**, 045901 (2015).
[35] S. Marsh, *LASL Shock Hugoniot Data* (University of California Press, Los Angeles, 1980).
[36] A. P. Hammersley, ESRF Internal Report No. ESRF97-HA02T (1997).
[37] A. P. Hammersley, S. O. Svensson, M. Hanfland, A. N. Fitch, and D. Hausermann, High Press. Res. **14**, 235 (1996).
[38] M. Hanfland, U. Schwarz, K. Syassen, and K. Takemura, Phys. Rev. Lett. **82**, 1197 (1999).
[39] M. I. McMahon, R. J. Nelmes, N. G. Wright, and D. R. Allan, Phys. Rev. B **50**, 739 (1994).
[40] N. Funamori and K. Tsuji, Phys. Rev. Lett. **88**, 255508 (2002).
[41] H. J. McSkimin and P. Andreatch, J. Appl. Phys. **35**, 3312 (1964).
[42] H. Olijnyk, S. K. Sikka, and W. B. Holzapfel, Phys. Lett. **103A**, 137 (1984).

[43] J. Z. Hu and I. L. Spain, Solid State Commun. **51**, 263 (1984).

[44] D. A. Young, *Phase Diagrams of the Elements* (University of California Press, Berkeley, 1991).

[45] S. M. Sharma and S. K. Sikka, Prog. Mater. Sci. **40**, 1 (1996).

[46] M. Mayo, S. Shor, E. Yahel, and G. Makov, J. Chem. Phys. **142**, 194501 (2015).